Spin-phonon coupling and magnetoelectric properties: $EuMnO_3$ versus $GdMnO_3$

W. S. Ferreira, J. Agostinho Moreira,* A. Almeida, M. R. Chaves, J. P. Araújo, J. B. Oliveira, J. M. Machado Da Silva, M. A. Sá, T. M. Mendonça, and P. Simeão Carvalho
Departamento de Física, IFIMUP and IN-Institute of Nanoscience and Nanotechnology, Faculdade de Ciências, Universidade do Porto, Rua do Campo Alegre, 687, 4169-007 Porto, Portugal

J. Kreisel
Laboratoire des Matériaux et du Génie Physique, CNRS, Grenoble Institute of Technology, 38016 Grenoble, France

J. L. Ribeiro and L. G. Vieira
Grupo FCD-Centro de Física, Universidade do Minho, Campus de Gualtar, 4710-057 Braga, Portugal

P. B. Tavares
Centro de Química, Universidade de Trás-os-Montes e Alto Douro, Apartado 1013, 5001-801 Vila Real, Portugal

S. Mendonça
Departamento de Física, INESC-Centro de Optoelectrónica e Lasers, Faculdade de Ciências, Universidade do Porto, Rua do Campo Alegre, 687, 4169-007 Porto, Portugal
(Received 8 October 2008; published 13 February 2009)

Correlation between spin-phonon coupling and the magnetoelectric properties of $EuMnO_3$ and $GdMnO_3$ were investigated using ceramic samples in this work. The experimental results evidence a stronger spin-phonon coupling in $GdMnO_3$ than in $EuMnO_3$, as well as a clear anomaly in the phonon contribution for the dielectric constant. This anomaly is located at the paramagnetic-incommensurate antiferromagnetic phase-transition temperature of $GdMnO_3$, corroborating the existence of a magnetoelectric effect in this system. The absence of the magnetoelectric effect in $EuMnO_3$ is due to the existing disorder revealed in this compound by the striking thermal metastability and the large decrease in the activation energy associated with the dielectric relaxation processes. This kind of behavior has no counterpart in $GdMnO_3$. In fact, it has been confirmed that the existence of spin-phonon coupling is not a sufficient condition for the existence of magnetoelectric property, and other mechanisms have to be considered in order to understand the magnetoelectric properties.

DOI: 10.1103/PhysRevB.79.054303 PACS number(s): 78.30.−j, 75.80.+q, 77.22.Gm

I. INTRODUCTION

In the last two decades, the search for materials that may exhibit magnetoelectric effect has drawn a renewed interest due to their great potential in emerging technological applications, as well as in the fundamental questions underlying their interesting physical behavior.[1,2]

It has been stressed, in current literature, the important role played by spin-phonon coupling for the onset of magnetoelectric effect. Although spin-phonon coupling has been observed in a large variety of materials exhibiting ferromagnetic (FM) and antiferromagnetic (AFM) orders, as well as in superconducting and magnetoresistive compounds, a magnetoelectric effect has not been observed in many of them.[3–7] Since the existence of spin-phonon coupling is not a sufficient condition for the existence of magnetoelectric effects, other mechanisms have to be considered in order to understand the coupling between magnetic and electric dipolar orderings.

In this regard, orthorhombic rare-earth manganites, $ReMnO_3$, with Re=Nd, Sm, Eu, Gd, Tb, and Dy, are interesting materials for the study of the correlation between spin-phonon coupling and the magnetoelectric effect, for they can be switched from nonmagnetoelectric to magnetoelectric by means of the tuning of the Mn^{3+} magnetic structure through changes of the rare-earth ionic radius.[8,9] The boundary, where this switching occurs, is filled by both $EuMnO_3$ and $GdMnO_3$. While the latter compound is magnetoelectric, presenting a magnetically induced polarization, the former is reported to be nonmagnetoelectric[9–12] even though these materials exhibit similar phase sequences. It is worth to stress that the different physical behavior exhibited by $EuMnO_3$ and $GdMnO_3$ stems from the different ionic radius of Eu^{3+} and Gd^{3+} and diverse electronic configuration of their $4f$ shells (Eu^{3+}:$^7F_0$; Gd^{3+}:$^8S_{7/2}$). In order to gain a better understanding of the mechanisms associated with the peculiar behavior of these compounds, we have carried out a systematic and comparative experimental study of their lattice dynamics, specific heat, dielectric, and magnetic properties. Our aim is to get information about (i) the relaxational processes involved in these compounds, (ii) the stability of the low-temperature magnetic phases, and (iii) the phonon contribution to the dielectric constant and the temperature behavior of the phonon frequencies in order to evaluate their role in regard to the existence of spin-phonon coupling and magnetoelectric effect and, in the case they are mutually dependent, how they are correlated in both $EuMnO_3$ and $GdMnO_3$.

Instead of making use of single crystals, as it is generally the case, we have performed our studies in ceramic samples processed by the sol-gel combustion method.[13] Despite their granular nature, ceramics allow to address the above objec-

tives and, furthermore, present the interest of allowing a systematic comparison between the behavior of single crystals and ceramics. Moreover, whenever practical applications are envisaged, ceramics are much more attractive due to their low cost, simpler, and fine-tuned-controlled preparation and versatility.

Let us summarize some of the physical properties of $EuMnO_3$ and $GdMnO_3$. At room temperature, both compounds are paraelectric (PE) and paramagnetic (PM) with a distorted perovskite structure of orthorhombic symmetry (*Pbnm*).[12,14] The two compounds undergo a phase transition to an incommensurate antiferromagnetic phase (ICAFM) at $T_N^{Eu} \sim 50$ K and at $T_N^{Gd} \sim 42$ K, with a modulation wave vector directed along the *b* axis.[10–12] This modulation corresponds to a collinear arrangement of the Mn^{3+} spins, and it is a consequence of competing exchange interactions between successive neighbor spins, which lead to a frustrated magnetic system. Both compounds undergo a further magnetic transition into an *A*-type antiferromagnetic order ($T_1^{Eu} \sim 43$ K and $T_1^{Gd} \sim 23$ K).[9,10,12,15] The observed weak ferromagnetism has suggested for both compounds a canted *A*-type antiferromagnetic ordering (cAAFM) of the Mn^{3+} spins along the *c* axis for $T < T_1$, but a direct magnetic structure determination has not been published yet.[8,16] Based on measurements of the thermal expansion and magnetostriction of $GdMnO_3$ along the three crystallographic axes, with applied magnetic field up to 14 T, a detailed study of the ICAFM/cAAFM phase transition was reported.[17] The feature of the phase diagram proposed is the downbending and the strong hysteresis of the ICAFM/cAAFM phase boundary at low magnetic fields, which has been interpreted by assuming a phase coexistence in the low-temperature and low-field range. A long-range order of the Gd magnetic moments has been put forward below $T_N^{Gd} \sim 5.1$ K.[10,15]

The ground state of $GdMnO_3$ is not ferroelectric (FE) in the absence of a magnetic field. However, by applying a rather low magnetic field ($\sim 10^4$ Oe) parallel to the *b* axis, a ferroelectric order is induced along the *a* axis.[14] Contradictory results have been reported for the FE polarization. Kuwahara *et al.*[18] found a finite polarization below 13 K, while Kimura *et al.*[10] observed a FE order only between 5 and 8 K, at low magnetic fields. The applied magnetic field seems to stabilize a commensurate magnetic structure below 15 K, with $\delta = 1/4$.[9,19]

II. EXPERIMENTAL DETAILS

The phase purity and the crystallographic characterization of the ceramic samples, processed through the sol-gel combustion method, were checked using x-ray powder diffraction and scanning electron microscopy. No secondary phases or significant deviation of the oxygen occupancy from the values expected for stoichiometric $ReMnO_3$ were observed for both samples. Scanning electron microscopy analysis reveals in both systems a typical ceramic microstructure with regular-shaped crystal grains ranging from 3 up to 10 μm in diameter. The mean grain size is about 6 μm.

The heat capacity was measured in an ARS Cryocooler, between 8 and 300 K, in a quasiadiabatic fashion by means of an impulse heating technique.

The samples used to perform the dielectric measurements have the form of a regular parallelepiped. Gold electrodes were deposited using the evaporation method. The complex dielectric constant was measured with an HP4284A impedance analyzer, in the 5–300 K temperature range and under an ac electric field of amplitude 1 V/cm for 10 KHz and 1 MHz.

Low-field dc induced specific magnetization measurements were carried out using commercial superconducting quantum interference device (SQUID) magnetometer in the temperature range 4–300 K.

The unpolarized Raman spectra were obtained with a T64000 Jobin-Yvon triple spectrometer, coupled to a liquid-nitrogen-cooled charge coupled device. The excitation line was the 632.8 nm of a He-Ne laser. The incident laser power was about 1 mW in order to avoid the local heating of the sample. Identical conditions were maintained for all scattering experiments. The spectral slit width was about 1.5 cm^{-1}. The samples were placed in a closed-cycle helium cryostat (10–300 K temperature range) with a temperature stability better than 0.5 K. The temperature of the sample was estimated to differ by less than 1 K from the temperature reading of a silicon diode attached to the sample holder. The Raman spectra were fitted with a sum of independent damped harmonic oscillators.[20]

The unpolarized infrared reflectivity measurements were performed with a Bruker IFS 66 V spectrometer. Room-temperature pyroelectric detectors of deuterated triglycine sulphate (DTGS) with polyethylene or KBr windows and Mylar 6 μ-M8 or KBr beam splitters were used to cover the spectral range 40–4000 cm^{-1}. The spectral resolution was better than 4 cm^{-1}. The complex dielectric function has been evaluated from the infrared (IR) data both by Kramers-Kronig inversion and by fitting the factorized form of the dielectric function.[21] Due to the difficulties raised by the complexity of the spectra and by the many overlapping reflectivity bands, we have imposed the condition of equal damping coefficients for longitudinal and transversal optical modes.

More details of the experimental techniques of the measurements of the dielectric constant, magnetization, Raman scattering, and infrared reflectivity spectra have been described in earlier Refs. 20–23.

III. EXPERIMENTAL RESULTS AND DISCUSSION

Figure 1(a) shows the specific heat C_p of $EuMnO_3$ as a function of temperature. Two anomalies are revealed at $T_N = 50$ K and at $T_1 = 43$ K. These values are in excellent agreement with those reported for the PM/ICAFM and ICAFM-cAAFM phase transitions in $EuMnO_3$ single crystals, respectively.[10–12]

The temperature dependence of the real (ε_r') and imaginary (ε_r'') parts of the dielectric constant measured at several frequencies is shown in Figs. 1(b) and 1(c). In general, the $\varepsilon_r'(T)$ curves agree well with the temperature behavior of the dielectric constant along the *a* axis (ε_a), reported by Goto *et al.*[9] The critical temperature of the PM/ICAFM phase transition cannot be directly obtained from the analysis of both

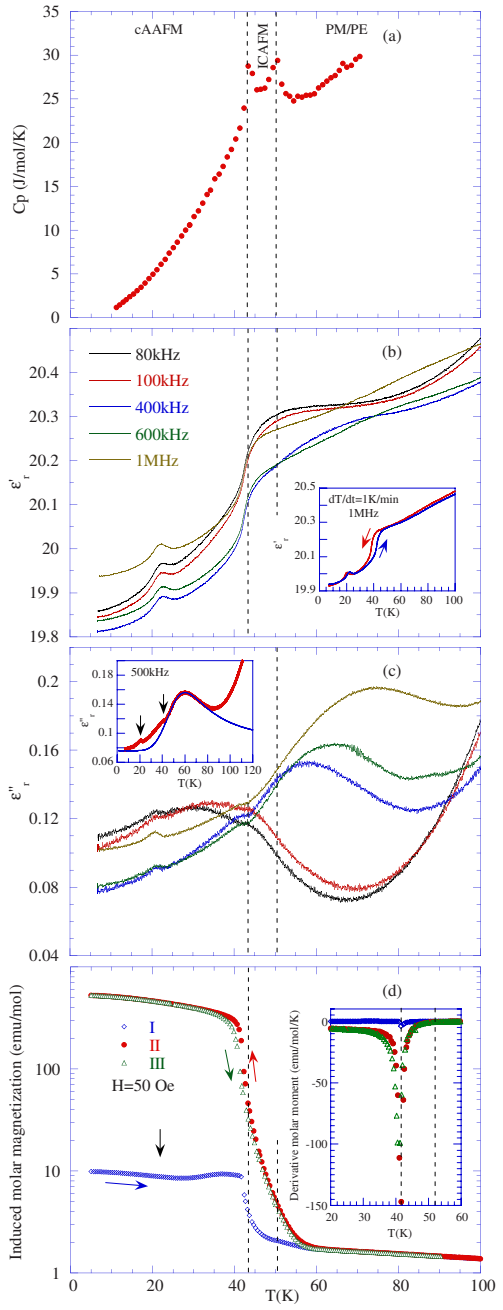

FIG. 1. (Color online) (a) Specific heat of $EuMnO_3$ as a function of the temperature. (b) Temperature dependence of the real part of the dielectric constant measured at various fixed frequencies. Inset: real part of the dielectric constant measured at 1 MHz in cooling and heating runs. (c) Imaginary part of the dielectric constant as a function of temperature measured at various fixed frequencies. Inset: imaginary part of the dielectric constant measured at 500 kHz; the vertical arrows signalize the anomalies observed in $\varepsilon_r''(T)$; the solid blue line represent the best fit of Eq. (1) (see text) to the experimental data. (d) Temperature dependence of the induced molar magnetization measured under an applied dc magnetic field of 50 Oe. Curve I: heating run after cooling the sample under zero-field; curve II: cooling run; curve III: heating run; the vertical arrow signalize the temperature where anomalous behavior in both $\varepsilon_r'(T)$ and $\varepsilon_r''(T)$ are observed. Inset: temperature derivative of the induced molar magnetization. The vertical dashed lines signalize the critical temperatures.

$\varepsilon_r'(T)$ and $\varepsilon_r''(T)$ curves, as it has also been observed in single crystals. $\varepsilon_r'(T)$ displays a steep decrease at around $T_1 = 43$ K followed by a second anomaly, which peaks at $T' = 23$ K. The amplitude of the steep decrease ($\Delta\varepsilon_r' \sim 0.3$) is of the same order of magnitude of that observed for single crystals ($\Delta\varepsilon_r' \sim 0.5$), and it marks the ICAFM-cAAFM phase transition. Thermal hysteresis in $\varepsilon_r'(T)$ is detected, corroborating the first-order character of the ICAFM-cAAFM phase transition [see inset of Fig. 1(b)]. $\varepsilon_r''(T)$ exhibits a broad anomaly, strongly dependent on frequency, and two anomalies at 43 and at 20 K, respectively, which are emphasized in the inset of Fig. 1(c). The maximum value of the broad feature shifts to lower temperatures as the frequency decreases.

Figure 1(d) shows the temperature behavior of the induced molar magnetization measured under an applied dc magnetic field of 50 Oe, in a heating run [curve (I)] after cooling the sample in zero field. Curves (II) and (III) give the induced molar magnetization measured in successive heating [curve (II)] and cooling runs, respectively. Above 60 K, the magnetization curves converge and follow a Curie-Weiss law, with a Curie temperature of $\theta = -88$ K. The obtained value of the effective paramagnetic moment is $6.7\mu_B$. Curve (I) and the inset of Fig. 1(d) show the temperature derivative of curves (I)–(III) as a function of the temperature. As the temperature increases from 5 K, the induced molar magnetization [curve (I)] decreases very slowly, reaching a local minimum at around $T' = 23$ K. On further heating, the induced magnetization slightly increases and reaches a maximum value at 39 K and then suddenly decreases. A sharp peak in the temperature derivative of the magnetization curve at $T_1 = 43$ K, marks the ICAFM-cAAFM phase transition. A small anomaly is observed at 52 K, associated with the PM-ICAFM phase transition. Regarding curves (II) and (III), in spite of a small thermal hysteresis of about 3 K below T_1 [visible in the inset of Fig. 1(d)], no significant difference is observed on entering or leaving out the low-temperature magnetic phases with an applied magnetic field. It is interesting to notice that the anomalous behavior in curve (I) occurring at near $T' = 23$ K is no longer observed in curves (II) and (III). The large difference between the saturation values of the induced molar magnetization shown in curve (I) and curves (II) and (III) is typically associated with disorder in the magnetic structure. Our results point out that competitive magnetic interactions of FM and AFM type may give rise to a disorder state in $EuMnO_3$. We will return to this issue below.

The anomalies observed at around $T' = 23$ K in both $\varepsilon_r'(T)$ and $\varepsilon_r''(T)$, and in the induced magnetization curve (I) are not shown in the specific heat. This anomaly is an intrinsic feature of $EuMnO_3$ crystals, and it should not be associated with the granular nature of our samples. In fact, Goto *et al.*[9] reported a small anomaly at 30 K in the temperature dependence of ε_a measured in single crystals. The absence of any detectable anomaly in the specific heat near T' points out that there is no contribution of the phonons to that anomaly. So the mechanism associated with such anomalous behavior in the temperature dependence of both the dielectric constant and induced magnetization should rather arise from a spin reorientation, which slightly reinforces the ferromagnetic component below T', as it can be seen in Fig. 1(d). Note that

we cannot exclude that this anomaly is connected with the onset of a novel nonstructural magnetic phase transition. Further experimental studies are still needed in order to test this possibility.

In the following we will consider the results obtained in $GdMnO_3$ ceramics. Figure 2(a) shows the specific heat as a function of temperature. A clear λ-like anomaly is found at $T_N \sim 42$ K, marking the onset of the ICAFM phase. Furthermore, a monotonous increase in C_p with decreasing temperature is observed below 12 K, which is likely associated with the ordering of the Gd^{3+} spins. The ICAFM-cAAFM phase transition is seen by a small anomaly in $C_p(T)$ around 17 K, shown in C_p/T curve displayed in the inset of Fig. 2(a). A more detailed analysis of the specific-heat data will be published elsewhere.

The $\varepsilon_r'(T)$ and $\varepsilon_r''(T)$ curves, measured at several frequencies, are displayed in Figs. 2(b) and 2(c), respectively. We observe a smooth step decrease in $\varepsilon_r'(T)$ and a broad anomaly in $\varepsilon_r''(T)$, over a large temperature range, occurring above 20 K. Between 20 and 100 K, the value of $\varepsilon_r'(T)$ does not change significantly (less than 2%) and the magnitude of the step anomaly decreases with decreasing frequency. The maximum value of $\varepsilon_r''(T)$ is strongly frequency dependent. Another anomaly in both $\varepsilon_r'(T)$ and $\varepsilon_r''(T)$ at around $T_1 = 14$ K is well detected, and a shoulderlike anomaly in $\varepsilon_r''(T)$ is also visible at $T_N = 42$ K [see inset of Fig. 2(c)]. No further anomalies in $\varepsilon_r'(T)$ and $\varepsilon_r''(T)$ are found below 10 K. A thermal hysteresis in $\varepsilon_r'(T)$ is observed below 20 K [see inset of Fig. 2(b)], in good agreement with the previous published results obtained in single crystals.[10] Unlike the case of $EuMnO_3$, the $\varepsilon_r'(T)$ profile in $GdMnO_3$ does not correspond to any of the dielectric constant curves measured along a specific crystallographic axis of the single crystals.[9] However, the value obtained for ε_r' on our ceramic samples agrees rather well with the average value of the dielectric constant along the three crystallographic directions, suggesting that the grains in the studied ceramic are randomly orientated.

Figure 2(d) shows the temperature dependence of the induced molar magnetization measured under an applied dc magnetic field of 50 Oe in a heating run [curve (I)] after cooling the sample under zero field. Curves (II) and (III) give the induced molar magnetization measured in successive heating [curve (II)] and cooling runs, respectively. Above 60 K, the magnetization curves follow a Curie-Weis law, with a Curie temperature of $\theta = -34$ K, in excellent agreement with the value reported for single crystals.[16] The value of the effective paramagnetic moment is $9.2\mu_B$, a value which is higher than the value obtained in $EuMnO_3$ apparently due to the Gd^{3+} spin contribution. As the temperature decreases, the induced magnetization increases. Below ~30 K, curve (I) becomes distinct from curves (II) and (III), which aside a very small thermal hysteresis exhibit similar temperature profiles. Curve (I) exhibit an anomaly around $T_N^{Gd} \sim 4.1$ K, associated with the ordering of Gd^{3+} spins. The magnetic response of this material to the applied magnetic field is dominated by the strong paramagnetism of the Gd^{3+} ion, which hinders the direct observation of the anomalies arising from the ordering of the Mn^{3+} spins at $T_1 = 14$ K. Therefore, we have studied the temperature dependence of the temperature derivative of curves (I)–(III). The inset of Fig. 2(d) shows the temperature derivative of the induced molar magnetization measured in the heating runs referred above, and $\varepsilon_r'(T)$ curves measured at 1 MHz in heating and cooling runs. At $T_1 = 14$ K, where the dielectric constant peaks, a small but clear change in the temperature behavior of the derivative of the induced moment is observed, marking the ICAFM-cAAFM phase transition. This value is found to be 9 K below the value reported for single crystals.[9,10] These anomalies observed at T_1 actually correspond to the slope change in C_p/T signalized by an arrow in the inset of Fig. 3(a).

The strong frequency dependence of the dielectric constant, also observed in single crystals, suggests the existence of a relaxational process in both systems. In this work, the study of the thermal dependence of the dielectric relaxation was carried out at fixed frequencies. The relaxation behavior in both compounds is better studied by fitting $\varepsilon_r''(T)$ with a Debye model with a single relaxation time, assuming an Arrhenius law:[24]

$$\varepsilon_r''(T) = \frac{\frac{1}{2}\Delta\varepsilon'}{\cosh\left[\frac{U}{k_B}\left(\frac{1}{T} - \frac{1}{T_M}\right)\right]}, \quad (1)$$

where $\Delta\varepsilon'$ is the dielectric strength, U is the activation energy associated to the dielectric relaxation process, k_B is the Boltzmann constant, and T_M is the temperature of the maximum value of $\varepsilon_r''(T)$. In the fitting procedure, we assume that the main temperature dependence in Eq. (1) comes from the argument of the hyperbolic function. In fact, as it can be seen in Figs. 1(b) and 2(b), the values of $\Delta\varepsilon'$ may be taken as temperature independent. By the fitting procedure we calculate the value of T_M for each frequency. The corresponding relaxation time is the inverse of that frequency. The insets of Figs. 1(c) and 2(c) show examples of the fitting procedure results. Figure 3 shows the relaxation time τ as a function of the inverse of the temperature for both compounds. A linear relation between $\ln(\tau)$ and $1/T$ for both $T > T_N$ and $T < T_N$ is observed. For $T < T_N$, a decrease in slope is observed for both compounds. This decrease is sharper in $EuMnO_3$ than in $GdMnO_3$. The values of the activation energy for $T > T_N$ are 20 and 18 meV for $EuMnO_3$ and $GdMnO_3$, respectively, whereas below T_N, we found 18 and 7 meV, pointing to a remarkable decrease in the activation energy for $EuMnO_3$ at the PM-ICAFM phase transition. No anomalous behavior was detected around T_1. With regard to the relaxation process observed in both compounds, we would like to point out that the activation energy does change at T_N, but its Debye character does not. $EuMnO_3$ exhibits the largest difference between the activation energy measured above and below T_N. So, for $T < T_N$, the height of the energy barriers in $EuMnO_3$ becomes smaller than in $GdMnO_3$, allowing for a thermal hopping dipolar disorder to emerge in the former compound. In this regard, their low-temperature magnetic phases are expected to have distinct physical characteristics.

The low-temperature magnetic phase transitions in both compounds have been considered to be of first order.[15,17] In order to investigate the metastability of the low-temperature magnetic phases in both compounds, we have measured the

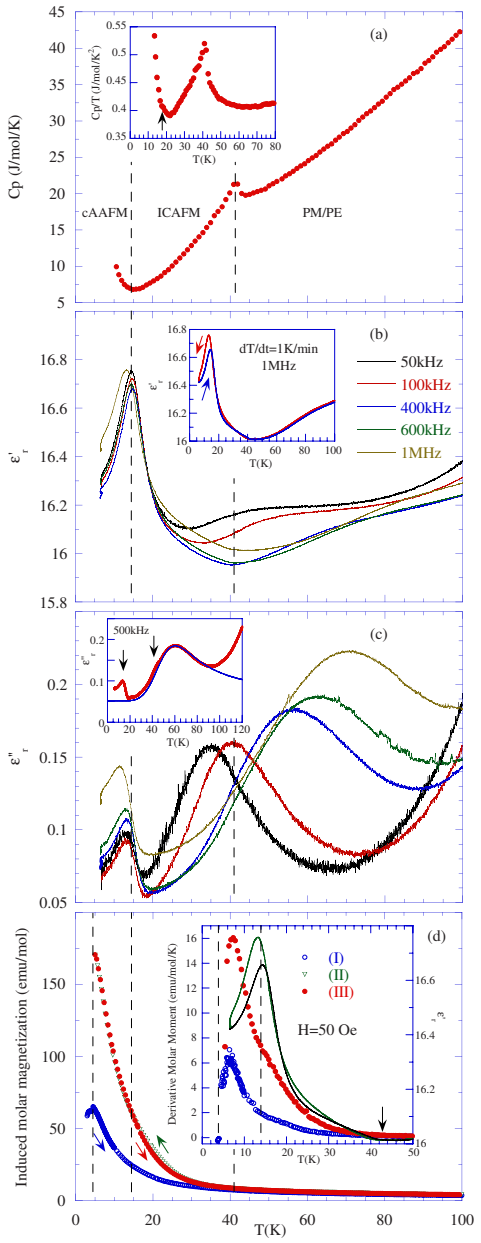

FIG. 2. (Color online) (a) Specific heat of $GdMnO_3$ as a function of the temperature. Inset: C_p/T as a function of the temperature. (b) Temperature dependence of the real part of the dielectric constant measured at various fixed frequencies. Inset: real part of the dielectric constant measured at 1 MHz in cooling and heating runs. (c) Imaginary part of the dielectric constant as a function of the temperature measured at various fixed frequencies. Inset: imaginary part of the dielectric constant measured at 500 kHz; the vertical arrows signalize the anomalies observed in $\varepsilon_r''(T)$; the solid blue line represent the best fit of Eq. (1) (see text) to the experimental data. (d) Temperature dependence of the induced molar magnetization measured under an applied dc magnetic field of 50 Oe. Curve I: heating run after cooling the sample under zero field; curve II: cooling run; curve III: heating run. Inset: temperature derivative of the induced molar magnetization and the temperature dependence of the real part of the dielectric constant measured at 1 MHz in heating and cooling runs; the vertical arrow signalizes the temperature of the PM-ICAFM phase transition. The vertical dashed lines signalize the critical temperatures.

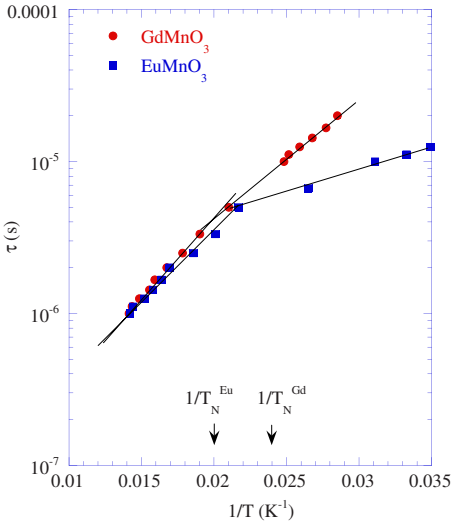

FIG. 3. (Color online) Relaxation time as a function of $1/T$ for $EuMnO_3$ (squares) and $GdMnO_3$ (circles).

dielectric constant at 600 kHz, using different temperature rates. Figure 4 shows the temperature dependence of the real part of the dielectric constant measured in heating and cooling runs at several temperature rates up to 8 K/min. As we can see, the $\varepsilon_r'(T)$ curve of $EuMnO_3$ is strongly dependent on the temperature rate and a large thermal hysteresis manifests in the heating and cooling cycles, in such a way that for a temperature rate of 8 K/min a thermal hysteresis of about 35 K is observed. Although the magnetic phase transitions in $GdMnO_3$ are also considered to be of first order, such an important thermal hysteresis is no longer observed. This issue cannot be thoroughly explained by just considering the first-order character of the magnetic phase transitions. On the contrary, it has to be understood in the scope of the emerging disorder referred above, where competitive interactions and phase coexistence are expected to play a major role in the low-temperature behavior of $EuMnO_3$.

Figures 5(a) and 5(b) show, respectively, the infrared reflectivity spectra of both $EuMnO_3$ and $GdMnO_3$ obtained at room temperature and at 20 K in the 40–700 cm^{-1} spectral range. We first observe that the spectral signature of $EuMnO_3$ and $GdMnO_3$ is very similar, which further confirms that both compounds adopt the same crystal structure. For the

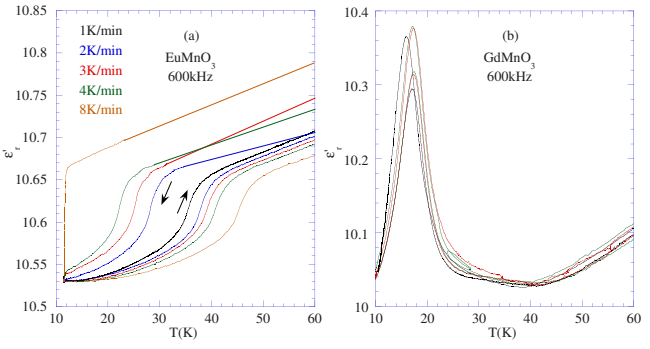

FIG. 4. (Color online) Temperature dependence of the real part of the dielectric constant of (a) $EuMnO_3$ and (b) $GdMnO_3$ measured in cooling and heating runs at several fixed temperature rates.

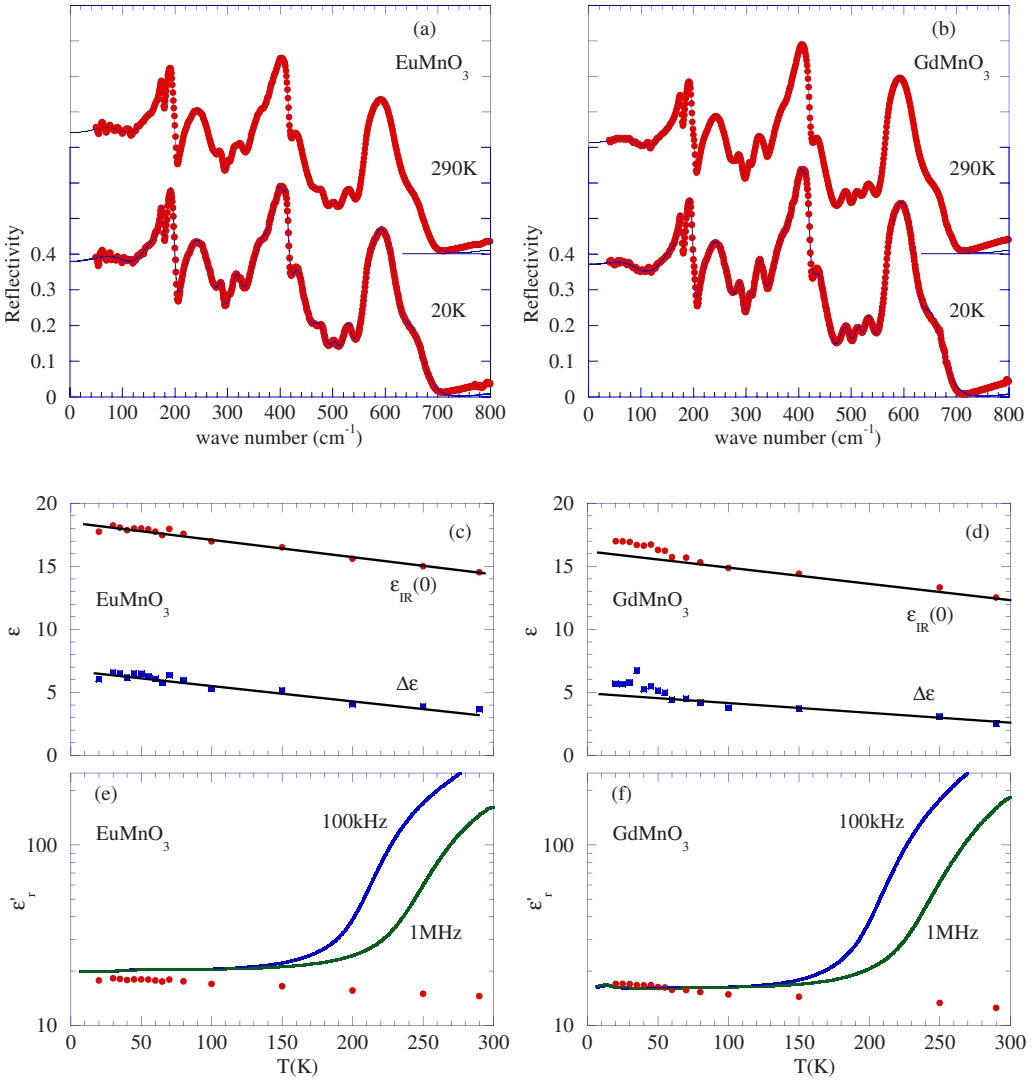

FIG. 5. (Color online) Infrared reflectivity spectra of (a) $EuMnO_3$ and (b) $GdMnO_3$ recorded at 290 and at 20 K. The solid blue lines represent the best fit of the factorized model of the dielectric constant to the experimental data. Low-frequency dielectric constant of (c) $EuMnO_3$ and (d) $GdMnO_3$ estimated from the reflectivity data [$\varepsilon_{IR}(0)$, red circles] and dielectric strength of the lower-frequency mode ($\Delta\varepsilon$, blue squares). Phonon (red circles) and the low-frequency (blue and green lines) contributions for the dielectric constant of (e) $EuMnO_3$ and (f) $GdMnO_3$.

Pbnm space group of orthorhombic $ReMnO_3$, a factor group analysis predicts $9B_{1u}+7B_{2u}+9B_{3u}$ infrared-active modes and $7A_g+7B_{1g}+5B_{2g}+5B_{3g}$ Raman-active modes. These modes are associated with three phonon bands which correspond to the normal modes of the ideal cubic perovskite: low-frequency external modes ($\omega<290$ cm^{-1}), bending phonon bands at intermediate range, and high-frequency stretching modes ($\omega>300$ cm^{-1}).[25] The external modes are due to Re and MnO_6 motion, while the bending and stretching modes are mainly due to oxygen vibrations. In addition, we observe in both compounds a broad and diffuse reflectivity band located within the range of the external modes, near 80 cm^{-1}.

Let us first consider the phonon contribution to the low-frequency dielectric constant. Because of the complexity of the spectra and the small changes observed, we have independently estimated this contribution from the fitting of the factorized form of the dielectric function to the reflectivity spectra and from the Hilbert transformation of the loss spectra calculated directly from Kramers-Kronig inversion of the reflectivity data. These two separate methods have provided consistent results that are shown in Figs. 5(c) and 5(d). As seen, in both compounds, the low-frequency dielectric constant estimated from the reflectivity data, $\varepsilon_{IR}(0)$, increases on cooling. A comparison between this function and the dielectric constant measured in the 10^6 Hz frequency range [see Figs. 5(e) and 5(f)] shows that, in the temperature range of the magnetic phase transitions, the low-frequency dielectric response is essentially due to the contribution of the polar phonons. This is consistent with the reduced strength of the relaxations detected in the 10^6 Hz frequency range. Unlike in $EuMnO_3$, we observe in $GdMnO_3$ a small anomaly in $\varepsilon_{IR}(0)$ near the transition to the modulated magnetic phase [see Fig. 5(d)], revealing that the incommensurate magnetic ordering affects the polar phonon response for the dielectric constant and hence leading to changes into its polar state.

The analysis of the temperature dependence of the vibrational parameters of the different phonon modes shows that the increase in $\varepsilon_{ir}(0)$ on cooling is essentially driven by the temperature dependence of the broad and diffuse mode observed near 90 cm^{-1}. Actually, all phonon modes above 100 cm^{-1} show residual temperature dependences of their dielectric strengths in both compounds. However, in the case of the lower-frequency mode, we observe an important increase in its strength on cooling. As seen in Figs. 5(c) and 5(d), in $EuMnO_3$ and $GdMnO_3$, its strength increases, respectively, from 4 and 3 at room temperature to 7 and 6 at $T=20$ K. For $GdMnO_3$, we also observe the steepest variation in the strength below $T\sim 50$ K, a temperature that correlates with the onset of a modulated spin structure. No anomalous behavior of the oscillator strength of the lower frequency mode in $EuMnO_3$ is detected.

It is not easy to ascribe the physical origin of the diffuse mode detected below 100 cm^{-1}. Pimenov *et al.*[26] reported the observation of an electric dipole active magnon in $TbMnO_3$ and $GdMnO_3$ in this frequency range. However, as the diffuse modes persist deeply into the high-temperature paramagnetic phase, we shall rule out this origin.

According to the mechanism proposed by Granado *et al.*,[5] one should expect detectable changes in the phonon frequencies on entering the magnetic phases, reflecting the expected phonon renormalization, proportional to the spin-spin correlation function for the nearest Mn^{3+} spins. In the case of $PrMnO_3$, $NdMnO_3$, and $SmMnO_3$, such an effect has been clearly seen by Raman spectroscopy, particularly in the high-frequency stretching vibrations of the oxygen atoms.[27] Surprisingly, it could not be found in the cases of $GdMnO_3$ and $EuMnO_3$.[27] In this class of compounds, the amplitude of the anomalies observed in the temperature dependence of the phonon frequencies at the magnetic ordering temperature is about 1–3 cm^{-1}. In order to get information concerning the coupling between spins and polar phonons, we have fitted the factorized form of the dielectric constant to the infrared reflectivity spectra. However, except for the well-resolved lattice mode located at $\sim$115 cm^{-1} (room-temperature value) in the spectra of $GdMnO_3$, the quantitative analysis of the infrared reflectivity spectra does not lead to definite results, preventing us to obtain accurate fit parameters in order to detect such small variations, due to the strong overlap of the reflectivity bands. Figure 6 depicts the wave number and the dielectric strength (right inset) of the referred polar lattice mode as a function of the temperature. The solid line was obtained from the best fit of the equation:[28]

$$\omega_j = \omega_{j0}\left(1 - \frac{c_j}{e^{\theta/T} - 1}\right), \qquad (2)$$

in the high-temperature range ($T>100$ K). In Eq. (2), ω_j is the frequency of the jth optical mode at the temperature T, θ is the Debye temperature, which is calculated from an average of the overall infrared active phonon frequencies, and ω_{j0} is the frequency of the jth mode at 0 K. The left inset of Fig. 6 shows the fit of the factorized form of the dielectric constant to the experimental data, in the relevant frequency range, at 290 and 20 K. The wave number increases as the temperature decreases and starts deviating from the high-

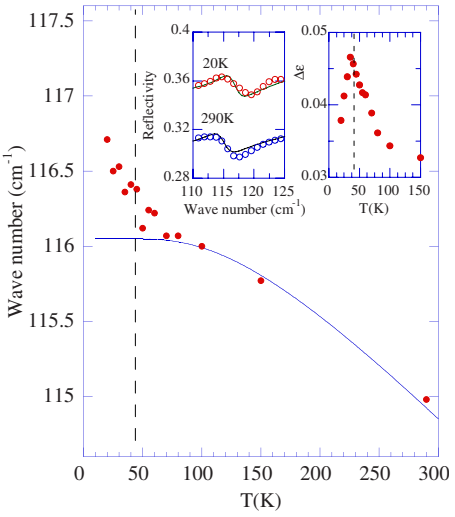

FIG. 6. (Color online) Temperature dependence of a polar lattice mode frequency of $GdMnO_3$. The solid line is obtained from the best fit of Eq. (2) (see text) to the experimental data for $T>100$ K. Insets: left: two examples of the fit of the factorized form of the dielectric constant to the experimental reflectivity data; right: temperature dependence of the dielectric strength.

temperature behavior at around 100 K. Moreover, its dielectric strength peaks at around T_N, suggesting that the onset of the incommensurate magnetic order affects the polar character of the lattice.

In order to figure out further spin-phonon couplings in $EuMnO_3$ and $GdMnO_3$, we have chosen to study the temperature dependence of the Raman bands associated with the MnO_6 symmetric (ν_s) and asymmetric (ν_{as}) stretching modes, as well as the corresponding bending (δ) and tilt (τ) modes. The referred Raman bands are well resolved in all temperature range studied, from which accurate fit parameters can be obtained. Figure 7 shows the Raman spectra of both $EuMnO_3$ and $GdMnO_3$ obtained at 290 and 9 K in the 300–700 cm^{-1} spectral range, together with a mode assignment of the most intense bands.

The temperature dependence of the Raman frequencies of the above referred normal modes is shown in Fig. 8. The solid lines in this figure correspond to the expected anharmonic temperature dependence of frequencies. These curves were obtained from the best fit to Eq. (2).

The mode frequencies increase as the temperature decreases from room temperature down to 100 K, in good

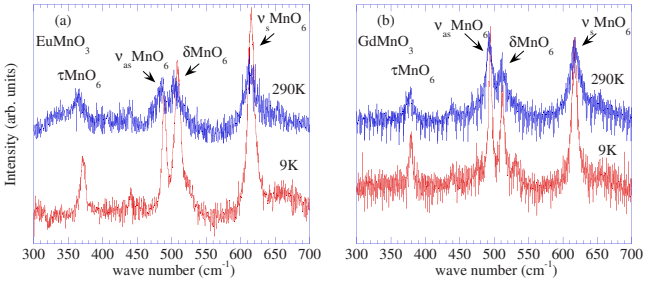

FIG. 7. (Color online) Raman spectra of (a) $EuMnO_3$ and (b) $GdMnO_3$ recorded at 290 and at 20 K.

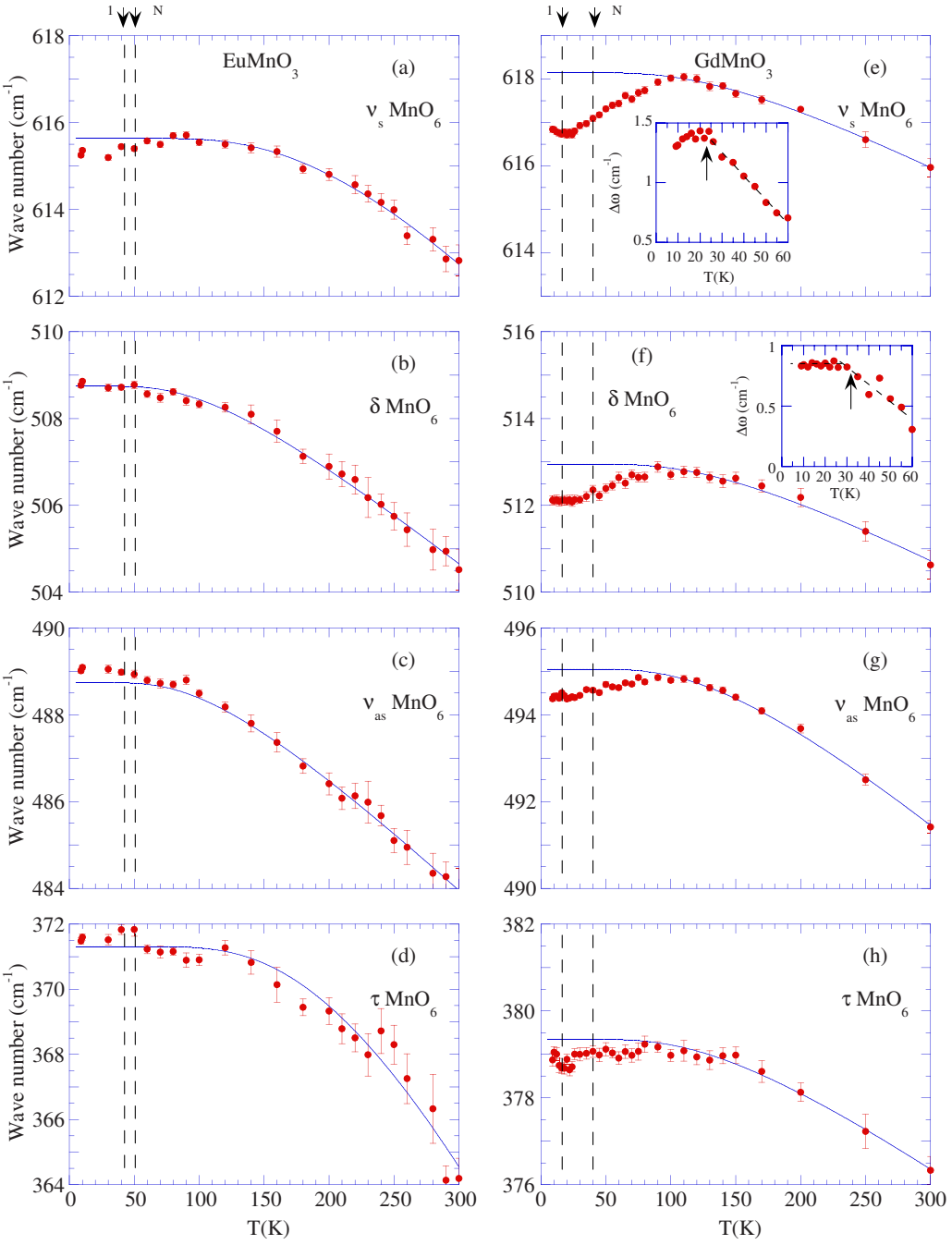

FIG. 8. (Color online) Temperature dependence of the Raman frequencies of $EuMnO_3$ [left frames (a)–(d)] and $GdMnO_3$ [right frames (e)–(h)]. The solid lines have been obtained from the best fit of Eq. (2) (see text) to the experimental data for $T > 100$ K. The insets show the temperature dependence of the frequency deviation from the extrapolated temperature behavior for $T > 100$ K. The error bars were estimated from the fit procedure.

agreement with the expected behavior arising from the anharmonic thermal contraction of the lattice. Below 100 K, a deviation from the extrapolated temperature behavior in the paramagnetic phase ($\Delta\omega$) is well observed for every mode of $GdMnO_3$, while for $EuMnO_3$ this deviation is smaller or even not visible. Among the Raman bands presented in Figs. 8(e)–8(h), the MnO_6 symmetric stretching mode displays the largest deviation. Its maximum value is ~ 1.5 cm^{-1}, occurring at around 20 K, close to the ICAFM-cAAFM phase-transition temperature $T_1 = 14$ K. The frequency of the bending mode also displays a clear deviation and a change in slope near 30 K, as it can be seen in the inset of Fig. 8(f).

The spin-phonon coupling in magnetic materials has been studied by several authors, and it was shown that the frequency shift of a given phonon mode as a function of the temperature can be described by taking into account the spin-spin correlation function:[7,29]

$$\omega = \omega_o + \gamma\langle \vec{S}_i \cdot \vec{S}_j \rangle, \quad (3)$$

where ω is the renormalized phonon frequency due to a spin-phonon coupling at a fixed temperature, ω_o denotes the frequency in the absence of this coupling, and γ is the coupling constant. Hence, in the magnetically ordered phase, an additional contribution to the phonon frequency is expected, arising from spin-phonon coupling. In our work, we have found deviations of the frequencies from the anharmonic high-temperature behavior above T_N. Such a kind of deviations has been also observed in a large number of other magnetic materials, providing evidence for the existence in these materials of a definite coupling between spins and phonons.[28]

IV. CONCLUSIONS

In this work we have presented a detailed study of dielectric relaxation processes, stability of the magnetic phases, the phonon dielectric response, and the spin-phonon coupling phenomena in both $EuMnO_3$ and $GdMnO_3$ ceramics. Regardless of the granular nature of the samples, our results provide evidence for similar intrinsic behavior of the ceramic samples and single crystals. In fact, there is a good agreement between the phase sequence and the critical temperatures in ceramics reported here and those for single crystals.[9] The magnitude of the dielectric constant and the induced magnetization in our ceramic samples are close to the average of the corresponding values measured in the different crystallographic directions of single crystals. Moreover, the unpolarized Raman spectra obtained in ceramics are the superposition of the spectra observed in different directions of single crystals.

The anomalies in the temperature dependence of the dielectric constant, which signalize the ICAFM-cAAFM phase transitions in $EuMnO_3$ and $GdMnO_3$ have different shapes providing clear evidence for a diverse behavior in regard to the coupling between magnetic and electric dipolar interactions. The relaxation time of the dielectric relaxation processes undergoes a distinct variation at the PM-ICAFM phase transition in $EuMnO_3$ and $GdMnO_3$, although smaller for the latter.

The experimental results obtained from the lattice dynamics studies show the existence of a coupling between spins and phonons in both compounds, much more pronounced in $GdMnO_3$. The polar phonon dielectric response of $GdMnO_3$ exhibits a clear anomaly at T_N, while in $EuMnO_3$ no significant variation is observed. Apparently, the increase in the polar character of the phonon response of $GdMnO_3$ below T_N has its origin in the deformation of the lattice, occurring above T_N. However, the lattice deformation might be very small as no net electric polarization is observed even by means of very precise pyroelectric measurements.[10] Nevertheless, due to the existing coupling between spins and the lattice, even a rather small magnetic field can give rise to large enough lattice deformations, which will lead to magnetically induced electric polarization, as it has been previously observed in $GdMnO_3$.[10]

The striking thermal metastability observed in $EuMnO_3$ by measuring the dielectric constant at different fixed temperature rates, as well as the large difference between the saturation values of induced molar magnetization, obtained under zero and nonzero applied magnetic field, show that the competitive exchange interactions between successive spins neighbors determine a large disorder of both spins and the electric dipolar momenta. This disorder could prevent the coupling between magnetic and electric dipolar orders, giving rise to a small coupling between spins and polar phonons. Therefore, the rising of an electric polarization in $EuMnO_3$ is not expected even under an applied magnetic field. Our results help to clarify why these two compounds presenting a similar phase sequences and magnetic structures, but very different spin-phonon coupling strength, behave so differently in what concerns the magnetoelectric effect.

ACKNOWLEDGMENTS

This work was supported by Fundação para a Ciência e Tecnologia through Project No. PTDC/CTM/67575/2006 and by Program Alßan, the European Union Program of High Level Scholarships for Latin America (Scholarship No. E06D100894BR). J.K. thanks the European STREP MaCoMuFi for financial support.

*jamoreir@fc.up.pt

[1] N. A. Spaldin and M. Fiebig, Science **309**, 391 (2005).
[2] M. Fiebig, J. Phys. D **38**, R123 (2005).
[3] J. Hemberger, T. Rudolf, H.-A. Krung von Nidda, F. Mayr, A. Pimenov, V. Tsurkan, and A. Loidl, Phys. Rev. Lett. **97**, 087204 (2006).
[4] J. Xu, J. H. Park, and H. M. Jang, Phys. Rev. B **75**, 012409 (2007).
[5] E. Granado, A. García, J. A. Sanjurjo, C. Rettori, I. Torriani, F. Prado, R. D. Sanchez, A. Caneiro, and S. B. Oseroff, Phys. Rev. B **60**, 11879 (1999).
[6] J. S. Lee, T. W. Noh, J. S. Bae, and T. In-Sang Yang, Phys. Rev. B **69**, 214428 (2004).
[7] D. J. Lockwood and M. G. Cottam, J. Appl. Phys. **64**, 5876 (1988).
[8] T. Kimura, S. Ishihara, H. Shintani, T. Arima, K. T. Takahashi, K. Ishizaka, and Y. Tokura, Phys. Rev. B **68**, 060403(R) (2003).
[9] T. Goto, T. Kimura, G. Lawes, A. P. Ramirez, and Y. Tokura, Phys. Rev. Lett. **92**, 257201 (2004).
[10] T. Kimura, G. Lawes, T. Goto, Y. Tokura, and A. P. Ramirez, Phys. Rev. B **71**, 224425 (2005).
[11] T. Arima, T. Goto, Y. Yamasaki, S. Miyasaka, K. Ishii, M. Tsubota, T. Inami, Y. Murakami, and Y. Tokura, Phys. Rev. B **72**, 100102(R) (2005).
[12] V. Yu. Ivanov, A. A. Mukhin, V. D. Travkin, A. S. Prokhorov, A. M. Kadomtseva, Yu. F. Popov, G. P. Vorob'ev, K. I. Kamilov,

and A. M. Balbashov, J. Magn. Magn. Mater. **300**, e130 (2006).
[13] C. Vázquéz-vázquez, M. Carmen Blanco, M. Arturo López-quintela, and D. Rodolfo, J. Mater. Chem. **8**, 991 (1998).
[14] K. Noda, S. Nakamura, J. Nagayama, and H. Kuwahara, J. Appl. Phys. **97**, 10C103 (2005).
[15] O. Ya. Troyanchuk and N. V. Kasper, Low Temp. Phys. **23**, 300 (1997).
[16] J. Hemberger, S. Lobina, H.-A. Krug von Nidda, N. Tristan, V. Yu. Ivanov, A. A. Mukhin, A. M. Balbashov, and A. Loidl, Phys. Rev. B **70**, 024414 (2004).
[17] J. Baier, D. Meier, K. Berggold, J. Hemberger, A. Balbashov, J. A. Mydosh, and T. Lorenz, Phys. Rev. B **73**, 100402(R) (2006).
[18] H. Kuwahara, K. Noda, J. Nagayama, and S. Nakamura, Physica B **359–361**, 1279 (2005).
[19] J. L. Ribeiro, Phys. Rev. B **76**, 144417 (2007).
[20] J. Agostinho Moreira, A. Almeida, M. R. Chaves, M. L. Santos, P. P. Alferes, and I. Gregora, Phys. Rev. B **76**, 174102 (2007).
[21] J. L. Ribeiro and L. G. Vieira, J. Phys.: Condens. Matter **18**, 7761 (2006).
[22] A. Almeida, J. Phys.: Condens. Matter **10**, 3035 (1998).
[23] C. Magen, P. A. Algarabel, L. Morellon, J. P. Araújo, C. Ritter, M. R. Ibarra, A. M. Pereira, and J. B. Sousa, Phys. Rev. Lett. **96**, 167201 (2006).
[24] C. J. F. Böttcher and P. Bordewijk, *Theory of Electric Polarization* (Elsievier, New York, 1978), Vol. 2.
[25] M. D. Fontana, G. Metrat, J. L. Servoin, and F. Gervais, J. Phys. C **17**, 483 (1984).
[26] A. Pimenov, T. Rudolf, F. Mayr, A. Loidl, A. A. Mukhin, and A. M. Balbashov, Phys. Rev. B **74**, 100403(R) (2006).
[27] J. Laverdière, S. Jandl, A. A. Mukhin, V. Yu. Ivanov, V. G. Ivanoc, and M. N. Iliev, Phys. Rev. B **73**, 214301 (2006).
[28] M. Balkanski, R. F. Wallis, and E. Haro, Phys. Rev. B **28**, 1928 (1983).
[29] W. Baltensperger and J. S. Helman, Helv. Phys. Acta **41**, 668 (1968).